

The effect of diffusion gradient direction number on corticospinal tractography in the human brain: an along-tract analysis

Claudia Testa^{1,2} · Stefania Evangelisti^{1,2} · Mariagrazia Popeo^{3,4} · Stefano Zanigni^{1,2} · Laura Ludovica Gramegna^{1,2} · Paola Fantazzini^{5,6} · Caterina Tonon^{1,2} · David Neil Manners^{1,2} · Raffaele Lodi^{1,2}

Received: 28 May 2016 / Revised: 17 November 2016 / Accepted: 23 November 2016 / Published online: 20 December 2016
© ESMRMB 2016

Abstract

Objectives We evaluated diffusion imaging measures of the corticospinal tract obtained with a probabilistic tractography algorithm applied to data of two acquisition protocols based on different numbers of diffusion gradient directions (NDGDs).

Materials and methods The corticospinal tracts (CST) of 18 healthy subjects were delineated using 22 and 66-NDGD data. An along-tract analysis of diffusion metrics was performed to detect possible local differences due to NDGD.

Results FA values at 22-NDGD showed an increase along the central portion of the CST. The mean of partial volume fraction of the orientation of the second fiber (f_2) was

higher at 66-NDGD bilaterally, because for 66-NDGD data the algorithm more readily detects dominant fiber directions beyond the first, thus the increase in FA at 22-NDGD is due to a substantially reduced detection of crossing fiber volume. However, the good spatial correlation between the tracts drawn at 22 and 66 NDGD shows that the extent of the tract can be successfully defined even at lower NDGD. **Conclusions** Given the spatial tract localization obtained even at 22-NDGD, local analysis of CST can be performed using a NDGD compatible with clinical protocols. The probabilistic approach was particularly powerful in evaluating crossing fibers when present.

Keywords Diffusion tractography · Corticospinal tracts · Healthy subjects

Electronic supplementary material The online version of this article (doi:10.1007/s10334-016-0600-1) contains supplementary material, which is available to authorized users.

✉ Raffaele Lodi
raffaele.lodi@unibo.it

¹ Functional MR Unit, Policlinico S. Orsola - Malpighi, Via Massarenti 9, Bologna, Italy

² Department of Biomedical and Neuromotor Sciences, University of Bologna, Via Foscolo 7, Bologna, Italy

³ Istituto Italiano di Tecnologia, Center for Neuroscience and Cognitive Systems@Unitn, Corso Bettini 31, Rovereto, Trento, Italy

⁴ Center for Mind and Brain Sciences, University of Trento, Corso Bettini 31, Rovereto, Trento, Italy

⁵ Department of Physics and Astronomy, University of Bologna, Viale Bertini Pichat 6/2, Bologna, Italy

⁶ Centro Enrico Fermi, Roma, Piazza del Viminale 1, Rome, Italy

Introduction

Tractography is a promising tool, which uses brain diffusion imaging data to investigate in vivo anatomical connectivity [1]. Apart from its role in the topographic localization of the major white matter fasciculi for the pre-operative planning, it has more recently been used to investigate non-invasively changes of diffusion properties of fiber paths in vivo [2, 3].

Starting from a set of seed points, probabilistic tractography characterizes the uncertainty in fiber path estimation, due to factors such as acquisition parameters or the presence of multiple fiber orientations per voxel, generating a large collection of possible trajectories. Brain regions that contain higher densities of these trajectories are considered to have a higher probability of connection with the seed point. It is possible to calculate the track density distribution with the seed mask for each voxel (i.e. the probabilistic

distribution of streamlines between that voxel and the seed mask) in addition to the evaluation of diffusivity tensor indices within the fiber tract.

In comparison, deterministic tractography delineates a unique trajectory that connects two regions of the brain [4, 5] assuming that the orientation of the longest axis of the diffusion tensor represents local fiber orientation. Thus, deterministic tractography may fail to identify tracts where white matter is characterized by crossing fibers [6].

Crossing fibers can also be identified using approaches based on spherical deconvolution integrated with either probabilistic or deterministic streamline algorithms for the estimation of fiber orientations [7, 8].

The variety and complexity of methods that have been developed for tractographic reconstruction can obscure the meaning of the underlying data, increasing the risk of misinterpreting the results [9, 10].

In a clinical context, the use of probabilistic reconstruction is less commonly preferred compared to deterministic approaches, partly due to computational limits, but also due to issues of data visualization. Recently, regional quantitative analyses of tractography data have been studied, since in the majority of tractography applications, results are limited to a visualization of the reconstructed tracts, yielding qualitative findings, or to an average evaluation of diffusion tensor measures (mainly mean diffusivity, MD, and fractional anisotropy, FA) over the entire tract, possibly missing localized changes in these more quantitative data. A few studies have investigated the regional quantification of diffusion parameters in white matter tracts [11–16] in order to detect differences between patients and control subjects in the diffusion properties of relevant tracts.

Different methods have been proposed to parameterize location within the tract under examination, such as the “angular coordinate” system [12] or the arc-length-based coordinate system [13, 15]. The interesting results presented by Oh et al. [16] demonstrate that the thalamo-frontal white matter tract shows an intra-subject variability along the tract significantly greater than inter-subject variability. This result confirms that a location-specific analysis of fiber bundles can be informative for studies of group comparisons.

The corticospinal tract (CST) is one of the principal tracts of the human brain involved in fine motor control and is frequently involved in events such as strokes and tumors, so the evaluation of changes in its microstructure is of particular interest. It is known from classical neuroanatomy studies that the CST arises in pyramidal neurons of the precentral gyrus, whose axons contribute to corona radiata formation and pass through the internal capsule where they are topographically arranged in the posterior limb. Corticospinal fibers traverse the middle portion of the

cerebral peduncle of the midbrain and then the basal pons [17]. Various techniques have been used to define the CST, some based on manually defined regions of interest (ROIs) [18, 19], others on voxel-based morphometry [20], or on an index of connectivity to define cortical areas as outlined by the Brodmann atlas connected with the internal capsule [2]. Here we propose a method to define ROIs for CST delineation which is semi-automatic and avoids the use of an atlas in order to make use only of subject-specific and group-specific anatomical information.

The effect of the number of gradient directions on derived diffusion measures was previously investigated [21–24] to derive an efficient scheme of acquisition and to determine the minimum number of gradient directions compatible with clinical applications and with an accurate evaluation of brain diffusion properties. Nevertheless, tractography results using different acquisition schemes have not previously been evaluated at a regional level in a clinical setting.

The goal of our study was to provide motivation for the choice of diffusion weighted imaging (DWI) protocols depending on the clinical application and on limitation of scan time. Given this aim, we examined how two different DWI protocols, differing in the number of gradient directions, influenced the definition of CST tract. We evaluated the results of an along-tract analysis of the CST delineated with a semi-automatic procedure using data obtained with the probabilistic tractography combined with the ball-and-stick model [25]. Specifically, we investigated whether DW acquisitions of healthy subjects with 22 and 66 diffusion gradient directions permitted reliable quantitative regional analyses of the CST by probabilistic tractography. By examining the extent and estimated diffusion parameters of the CST along the tract, the relative capabilities of the two acquisition protocols can be better understood, and an appropriate choice can then be made depending on the current clinical question, balancing the need to have the most accurate definition of the CST tract with the need to estimate the properties of the CST tract using a brief MR acquisition.

Materials and methods

Subjects

Eighteen healthy adult subjects (10 male and 8 female), with a mean \pm standard deviation (SD) age of 33 ± 12 years (range 23–69 years), were recruited by the Functional MR Unit, Department of Biomedical and Neuromotor Sciences of the University of Bologna, from among hospital and university workers and their relatives. All acquisitions were performed in September 2016. A

current or past history of neurologic or psychiatric disorders and major brain injuries was excluded in all participants by a neurologist (CaT, RL). Fourteen subjects were right-handed based on the Edinburgh Handedness Inventory [26], and four were left-handed. The protocol was approved by the local ethics committee and written informed consent was obtained from all individual participants included in the study.

MRI protocol

MR studies were performed using a 1.5 T (Signa HDx 15, General Electric Medical Systems Milwaukee, WI, USA) system equipped with a quadrature birdcage head coil. In all recruited participants a T_1 -weighted axial volumetric image was acquired using the FSPGR (fast spoiled gradient echo) sequence (TI = 600 ms, TE = 5.1 ms, TR = 12.5 ms, 25.6 cm² FOV, 1 mm isotropic voxels). For each subject axial diffusion weighted images were acquired using a single-shot SE-EPI (spin echo–echo planar imaging) sequence with TE = 80.6 ms, TR 12 s, FOV = 32 × 32 cm, data matrix = 128 × 128, 3 mm-thick contiguous slices, using b value = 1000 s mm⁻². Four separate DWI acquisitions were obtained, to vary the number of diffusion gradient-encoding directions while holding all the other parameters constant. The first three scans were identical, with 22 diffusion-weighted directions and three unweighted scans (22-NDGDs). The last scan was with 66 diffusion-weighted directions and 9 unweighted scans (66-NDGDs). All the 22-NDGD and 66-NDGD scans were performed in the same scanning session without moving the subject. The DWI acquisitions lasted 5 min 12 s for 22-NDGDs and 15 min 12 s for 66-NDGDs respectively.

Data processing

Preprocessing of data, diffusion tensor imaging (DTI) processing and tractography evaluation were performed using the FMRIB software library (<http://www.fmrib.ox.ac.uk/fsl>).

All 22-NDGD acquisitions were aligned using a rigid-body registration to the first volume of the first scan as reference in order to perform an average of both the unweighted volumes (3 in each 22-NDGD scan) and the weighted volume (22 in each 22-NDGD scan). This allowed data to be generated with 22-NDGDs, but with a signal-to-noise ratio (SNR) comparable with the 66-NDGD scan. We referred to this data as the $\overline{22}$ -NDGD data. We checked the SNR of $\overline{22}$ -NDGD unweighted volumes and 66-NDGD unweighted volumes: signal was evaluated over a mask of the brain and it was divided by the standard deviation of noise from a ROI drawn outside of the brain.

Diffusion echo planar (EP) images were corrected for eddy current effects using affine registration to a reference volume. Parameter maps for mean diffusivity (MD), fractional anisotropy (FA), longitudinal diffusivity (i.e. λ_1 , λ_2 , and λ_3) were determined voxel-wise using DTIFIT.

Given that T_1 -weighted volumetric images and diffusion images differ in both contrast and acquisition resolution, they were co-registered indirectly. For each subject an EP image (the synthetic image) was calculated based on a nonlinear combination of λ_1 , λ_2 , λ_3 maps and with contrast proportional to a T_1 -weighted image (Supporting Figure S1 and Supporting Table). Then, the T_1 -weighted volumetric image was aligned by FLIRT [27] to the synthetic image, and the synthetic image was unwarped to the aligned volumetric image in the image plane with a nonlinear transformation, using the ART software package [28].

All the voxel-wise maps of diffusion tensor parameters (MD, FA, λ_1 , λ_2 and λ_3) were then recalculated in the space of the synthetic image. For each subject, diffusion parameters map images were calculated at 66 NDGDs, at $\overline{22}$ -NDGDs and at 22-NDGDs.

In order to prepare data for tractography, the *bedpostx* algorithm (Bayesian Estimation of Diffusion Parameters Obtained Using Sampling Techniques), which is based on the ball-and-stick model, was applied [25]. *Bedpostx* allows the most appropriate number of multiple fiber orientations for the data to be assessed at each voxel. White matter tracking was then conducted by *probtrackx2* (http://fsl.fmrib.ox.ac.uk/fsl/fsl-4.1.9/fdt/fdt_probtrackx.html). The algorithm computes a probabilistic streamline by proceeding through samples drawn from the distributions of voxel-wise principal diffusion directions, to generate a sample from the distribution on the location of the true streamline. By taking many such samples, *probtrackx* builds up the histogram of the posterior distribution on the streamline location, or the connectivity distribution, thereby estimating the specific white matter tract from user-specified seed voxels. All brain voxels are characterized by a number, representing the connectivity value between that voxel and the seed voxels (the number of samples that pass through that voxel).

ROI definition and CST tractography

To delineate the CST in each subject, we defined the ipsilateral precentral gyrus, posterior limb of the internal capsule (PLIC), and pons in both brain hemispheres as ROIs. We also used an exclusion mask corresponding to the mid-sagittal plane in order to guarantee that the tract remains ipsilateral to the ROIs. The precentral gyrus was used as a seed mask while the PLIC and the pons defined waypoints reflecting the normal anatomical course of the CST tract.

- The precentral gyrus was delineated for each subject performing a grey matter segmentation of T_1 -weighted volumetric images, using Freesurfer [29]. After parcellation, masks of the precentral gyrus were registered to the *synthetic image* applying the previously performed transformation from the volumetric space to the *synthetic image* (Supporting Figure S2A).
- To ensure that both the PLIC and the pons were defined in the same way for each subject, we created a study-specific FA template. Every FA image was aligned to every other one, identifying the “most representative” one, which was used as the target image. The latter was then affine-aligned into MNI152 standard space and every FA image was aligned to the MNI152 space by combining the nonlinear transform to the target image with the affine transform from the target to MNI152 space [30]. We manually drew PLIC and pons onto the mean FA template and back-projected the results to individual DWI volumes. To project all subjects’ FA data onto a mean common space, we used the TBSS algorithm (tract-based spatial statistics), developed to perform voxelwise statistical analysis of FA data, and described in detail elsewhere [30]. ROIs of the pons, PLIC and the exclusion mask were drawn on the mean FA template by a neurologist expert in neuroimaging (SZ) (Supporting Figure S2b, S2c). Using the inverse of the transformation obtained by TBSS, ROIs were projected back to the original FA maps for each subject.

We delineated the CST for both sides of the brain at 22, at $\overline{22}$ and 66 NDGDs using *probtrackx2*. The algorithm drew 5000 samples going from each voxel in the precentral region to the waypoint masks. The output was a probabilistic map that provided a number for each voxel, the connectivity value, which corresponds to the number of samples that leave the precentral gyrus and go through the PLIC and the pons, discarding pathways which enter the exclusion mask. The algorithm also returns a number, the *waytotal*, that corresponds to the total number of generated tracts that have not been rejected by the exclusion mask.

Probabilistic tractography analysis

For inter-subject comparison, the connectivity maps of CST were normalized by dividing the connectivity values by the *waytotal*. Maps of 22-NDGD data were not thresholded, maps of $\overline{22}$ -NDGD were thresholded at 5×10^{-4} and those of 66-NDGD were thresholded at 2.5×10^{-4} to remove voxels whose locations were not likely to correspond to the CST and which can be considered to represent the effect of image noise. The thresholds were not equal because different NDGD tracts were characterized by different connectivity values [2, 31, 32]. The thresholded

connectivity maps were then used to mask the FA, MD, λ_1 , λ_2 , and λ_3 maps; then the mean of partial volume fraction estimates of orientations of both the first (f1) and the second fiber (f2) revealed by *bedpostx* were masked to analyze the differences between 22 and $\overline{22}$ -NDGD and the differences between $\overline{22}$ -NDGD and 66-NDGD data in detail. In particular, the volume of the principal fiber and of the second fiber if present (or given value zero if absent) were evaluated.

For both sides of brain, each tract was divided into 100 segments of equal length (percentiles) from the pons to the precentral gyrus (Supporting Figure S.3).

To investigate the spatial correspondence of the CST, as delineated at 22-NDGD, $\overline{22}$ -NDGD and at 66-NDGD, we calculated the 2D spatial correlation between tracts with 22- and $\overline{22}$ -NDGD and with $\overline{22}$ -NDGD and 66-NDGD at the level of each percentile. We also considered the coordinates of the centre of gravity (COG) for the binarized tract along left–right and anterior–posterior directions. In general, the COG corresponds to first moment of the spatial distribution of the tract, where the weight is the image intensity. In this case, given the binarization of the tract, the COG simply corresponds to the location of the average of the coordinates of the tract at the level of each percentile ($x_{COG} = \frac{\sum_{i=1}^N x_i}{N}$; $y_{COG} = \frac{\sum_{i=1}^N y_i}{N}$). To evaluate visually the spatial distribution of the tract, we created an image given by the sum of tract volumes of all subject in the space of the mean FA template.

Statistical analysis

Statistical analyses were conducted with SPSS (Statistical Package for the Social Sciences, version 21), JMP 10.0 (SAS Institute Inc.) and MATLAB (version 7.11). A *t* test was performed to test whether SNR was significantly different at $\overline{22}$ -NDGDs and 66-NDGDs. The Kolmogorov–Smirnov test was performed to test whether diffusion metrics were normally distributed.

The median value of FA, MD, λ_1 , λ_2 , λ_3 , f_1 volume and f_2 volume for each percentile was calculated since values had a non-Gaussian distribution. The relative contribution of inter- and intra-subject variability to the total observed variability for each parameter was examined as follows. A restricted maximum likelihood (REML) model of each data set was made considering subject and percentile as random factors. Percentiles above the 90th were ignored due to parameter estimation problems in the last slices (described below). The model partitioned variance into three components, namely along tract variance common to all subjects (common intra-subject variability), mean parameter value for each subject (inter-subject variability), and a residual term reflecting inter-subject differences only at specific points along the tract.

Two-way repeated measures analysis of variance (RMANOVA) was applied to determine side and NDGD ($\overline{22}$ -NDGD vs 66-NDGD) effect on FA, MD and waytotal.

Paired t tests were performed along the parameterized tracts for each subject, to individuate region-specific differences for side and NDGD effect. For each percentile, we performed a paired t test and the false discovery rate (FDR) method for multiple comparison correction was applied. The paired t tests were performed for all the diffusion metrics, FA, MD, λ_1 , λ_2 , λ_3 , and also for the volume corresponding to f_1 and f_2 .

The 2D and 3D spatial correlations of CST between 22-NDGD $\overline{22}$ -NDGD and between $\overline{22}$ -NDGD and 66-NDGD were calculated, in MATLAB, by the 2D Pearson Correlation and the Dice coefficient respectively.

Results

Image quality was good and no EPI image slices were discarded.

SNR measurements made on the unweighted images were not significantly different between $\overline{22}$ -NDGDs and 66-NDGDs (mean SNR was 134 and at $\overline{22}$ -NDGDs and 132 at 66-NDGDs, $p = 0.26$).

Figure 1 shows the CST tracking obtained following the procedure described. The 66-NDGD data (bottom) reveal a higher value of connectivity and projections to lateral portions of the sensorimotor strip that are less evident at $\overline{22}$ -NDGDs (middle) and at 22-NDGDs (top). An expanded view of the CST tract at level of the left corona radiata shows the superposition of crossing fiber bundles. In particular, the 66-NDGD data better identify the lateral motor projections (red) crossing the principal population of fibers (oriented superior-inferiorly). Distributions of median value of FA and MD are reported in Fig. 2 (panels a and b, respectively), for the right (top of each panel) and left side of brain (bottom of each panel) at 22-NDGD, $\overline{22}$ -NDGDs and 66-NDGDs (left, middle, right column, respectively). FA median values vary along the tract, with a similar pattern found in all the participants. MD values are constant

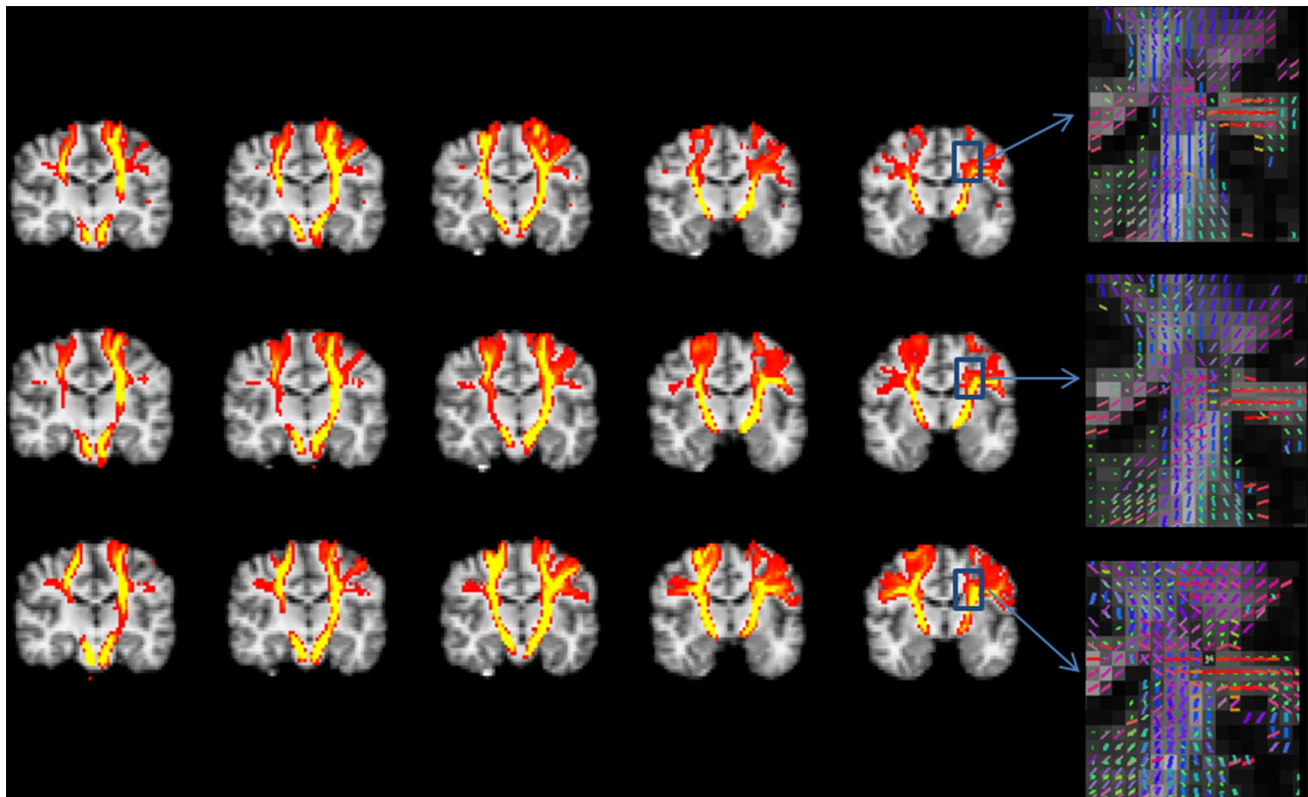


Fig. 1 Tracking the corticospinal tract (CST) from the precentral gyrus to the posterior limb of internal capsule and the pons at 22-NDGD (top), $\overline{22}$ -NDGD (middle) and 66-NDGD (bottom) in successive slices of a coronal view of one subject. Normalized and thresholded connectivity distribution of the right and left CST are superimposed onto the 3D T_1 -weighted image. Voxel are color coded from

10^{-4} (red) to 0.008 (yellow) samples passing through the voxel. At the right the area of the CST tract at level of the left corona radiata is enlarged to show the superposition of crossing fiber bundles. Mean direction vectors of the posterior distribution samples are shown, color-coded using normal DTI convention so that dominant fibers are red (inferior-superior) and second fibers are blue (left-right)

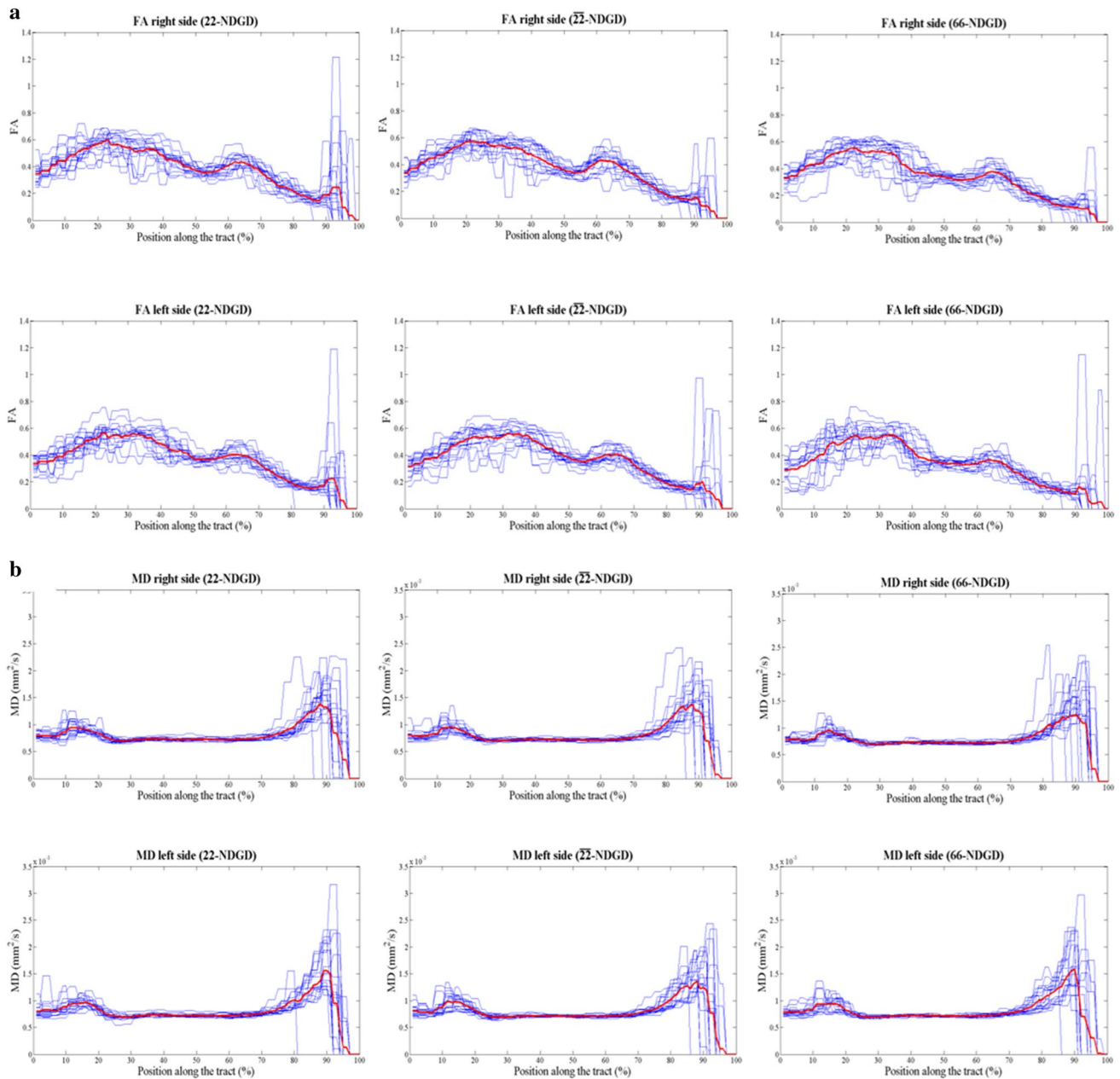


Fig. 2 Plot of median value of FA (**a**) and MD (**b**) for each percentile at 22-NDGD (first column), $\overline{22}$ -NDGD (second column) and 66-NDGD (third column), in each subject (blue lines) for the right

side of the brain and for the left side of the brain. Red line represents average values between subjects along the tract

until the 85th percentile, but in the upper part of the tract MD values show a great variability at each NDGDs.

An evaluation of intra-subject and inter-subject parameter variance, considering separately left and right sides and 22, $\overline{22}$ -NDGDs and 66 NDGDs was performed; the results are reported in Table 1

The residual variances of FA and MD values, corresponding to differences present only in certain portions of

the tract were significantly higher than inter-subject variances. In addition, the residual variances of both FA and MD are higher at 22-NDGDs with respect to $\overline{22}$ -NDGDs and 66-NDGDs.

Kolmogorov–Smirnov testing showed that FA, MD, and waytotal were normally distributed.

Descriptive statistics for FA, MD waytotal are reported in Table 2, along with the results of an RMANOVA test

Table 1 REML estimation of partition of variance for fractional anisotropy (FA), mean diffusivity (MD)

Effect	Common intrasubject variability, %	Whole tract intersubject variability, %	Residual variability, %
FA			
22-NDGD			
Right	64.0	9.1	26.9
Left	66.1	6.6	27.4
$\overline{22}$ -NDGD			
Right	68.1	7.6	24.3
Left	67.8	5.3	26.9
66-NDGD			
Right	65.5	8.8	25.7
Left	61.2	5.7	33.2
MD			
22-NDGD			
Right	40.9	4.5	54.7
Left	50.9	5.5	43.5
$\overline{22}$ -NDGD			
Right	48.9	6.0	45.0
Left	57.8	5.2	37.0
66-NDGD			
Right	45.8	3.8	50.3
Left	53.8	4.7	41.5

NDGD number of diffusion gradient directions

Table 2 Descriptive statistics (top) and results of RMANOVA (bottom) for FA, MD, and waytotal

Descriptive statistics (mean \pm SD)		FA	MD ($\times 10^{-3}$ mm ² s ⁻¹)	Waytotal ($\times 10^4$)		
$\overline{22}$ -NDGD						
Right		0.36 \pm 0.03	0.78 \pm 0.03	1.40 \pm 1.21		
Left		0.36 \pm 0.03	0.78 \pm 0.04	2.04 \pm 1.90		
66-NDGD						
Right		0.33 \pm 0.03	0.78 \pm 0.04	4.02 \pm 5.02		
Left		0.33 \pm 0.03	0.79 \pm 0.05	2.34 \pm 1.91		
RMANOVA	FA	MD		Waytotal		
	<i>F</i>	<i>p</i>	<i>F</i>	<i>p</i>	<i>F</i>	<i>p</i>
Effects						
Side	0.37	0.55	0.60	0.45	0.60	0.45
NDGD	31.60	<0.001	0.68	0.42	5.14	0.037

Significant results ($p < 0.05$) are reported in bold

NDGD number of diffusion gradient directions

using brain hemisphere and NDGD as factors. No effects of the brain side were found, while NDGD was found to affect FA and waytotal, but not MD. Waytotal variability was substantial, reflecting anatomical and “trackability” differences between subjects.

Along-tract analysis

Results of the paired t test for FA, and MD, considering as pairing parameters either brain hemisphere or NDGD, are shown in Figs. 3, 4. Differences that manifest in less than

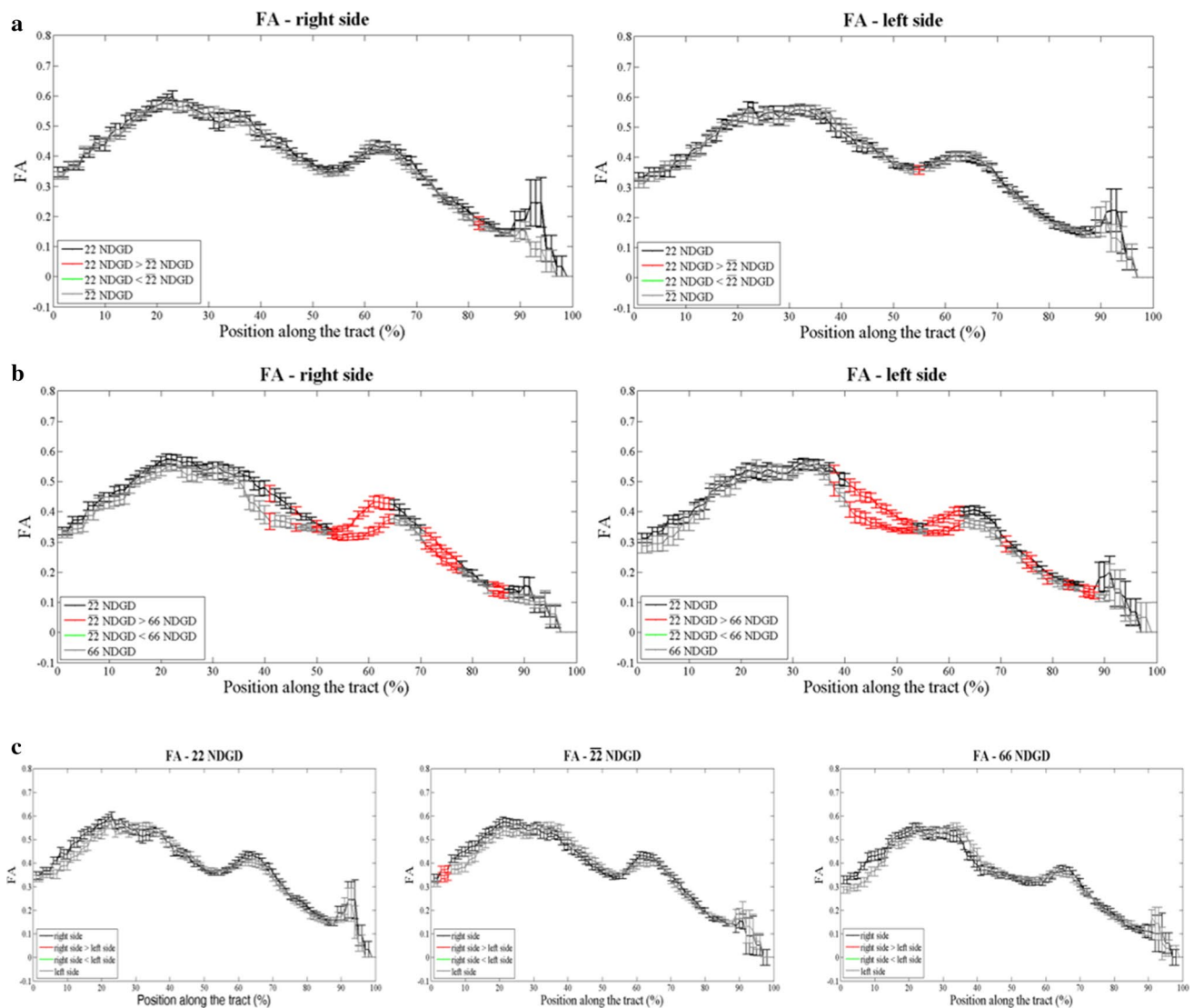


Fig. 3 Paired *t* test of FA. From the *top*, **a** illustrates FA distributions and differences between two NDGD (respectively 22 and 22) on given side (*right* and *left* etc). *Black line* represents FA at 22-NDGD and *grey line* at $\overline{22}$ -NDGD on given side (respectively *right* and *left*). *Red lines* indicate values at 22-NDGD which are higher than those at $\overline{22}$ and *green lines* indicate the opposite. **b** Illustrates FA distributions and differences between $\overline{22}$ -NDGD and 66-NDGDs. *Black line* represents FA at 22-NDGD, and *grey line* at 66-NDGD on given

side (respectively *right* and *left*). **c** Differences between sides of brain (*right* and *left*) for given NDGD (22, $\overline{22}$ and 66). *Black line* represents the right side and *grey line* the left side of the brain for given NDGD (respectively 22 on the *left*, $\overline{22}$ in the *middle* and 66 on the *right*). *Red lines* indicate values in the *right side*, which are higher than in the *left side* and *green lines* indicate the opposite. Differences are considered significant at $p < 0.05$ correcting using FDR

three consecutive percentiles correspond to a single significant comparison and are not considered relevant, as the distance between percentiles is roughly one third of the slice thickness).

Comparing acquisition strategies, FA appeared to be elevated along the central portion of the CST at the level of the PLIC, using $\overline{22}$ -NDGDs compared to 66 NDGDs (Fig. 3b), from the 50th to the 75th percentile on the right side (Fig. 3b, left) and from the 40th to the 60th percentile (from PLIC to corona radiata) on the left

side. No significant differences were found in three consecutive percentiles comparing 22-NDGDs to $\overline{22}$ -NDGDs (Fig. 3a). Figure 3c shows a small portion of tract (from 3rd to 5th percentile at level of the pons) with a higher FA at right found at $\overline{22}$ -NDGDs. MD was not significantly different both in the comparisons between 22-NDGDs and $\overline{22}$ -NDGDs (Fig. 4a) or between $\overline{22}$ -NDGDs and 66-NDGDs. Figure 4c shows no significant difference in MD values comparing left with right side at each NDGDs comparison.

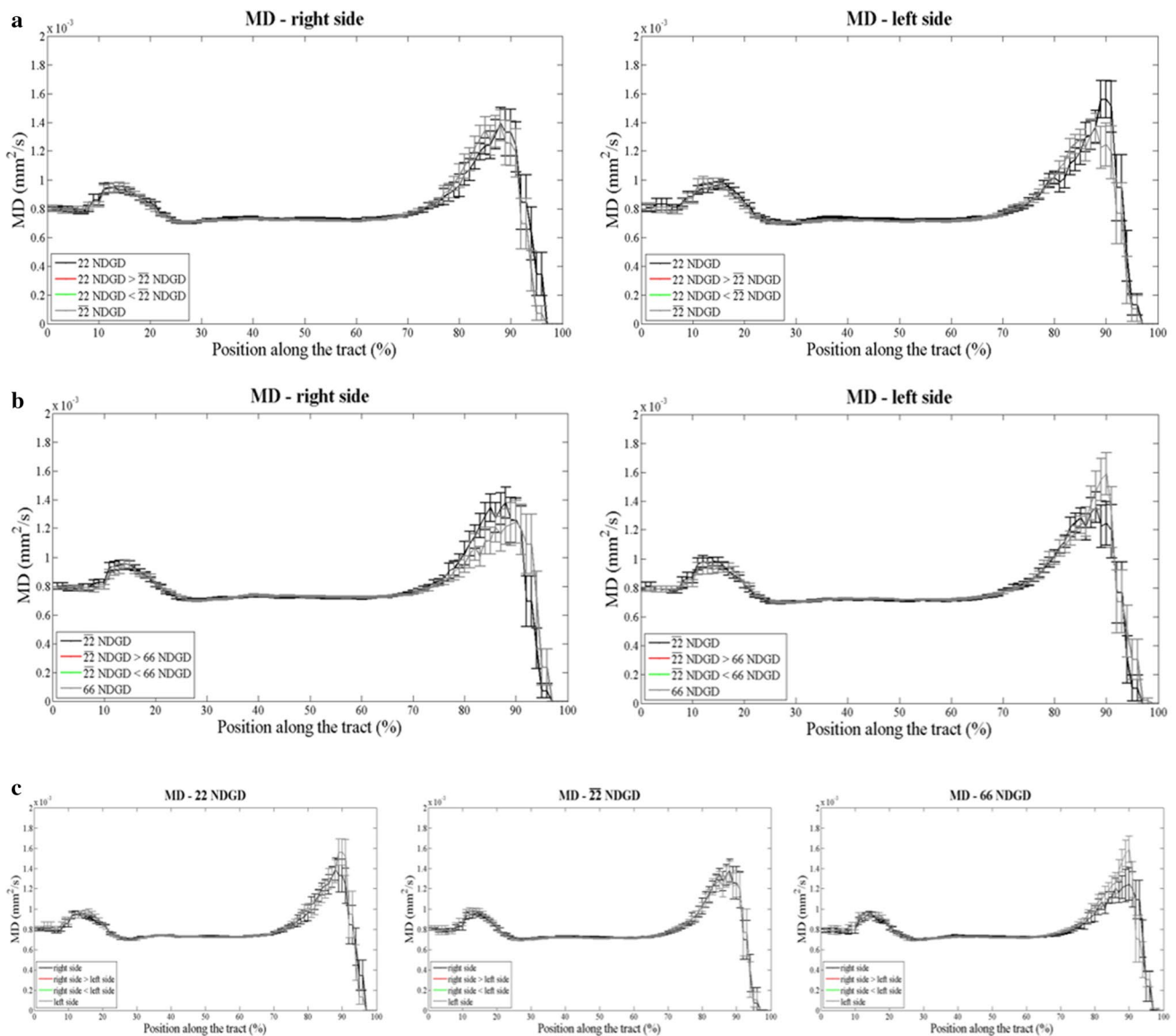


Fig. 4 Paired t test of MD. From the *top*, **a** illustrates MD distributions and differences between two NDGD (respectively, 22 and $\overline{22}$) on given side (*right* and *left*). *Black line* represents MD at 22-NDGD, and *grey line* at $\overline{22}$ -NDGD on given side (respectively *right* and *left*). *Red lines* indicate values at 22-NDGD which are higher than those at $\overline{22}$ and *green lines* indicate the opposite. **b** Illustrates MD distributions and differences between $\overline{22}$ -NDGD and 66-NDGDs. *Black line* represents MD at $\overline{22}$ -NDGD, and *grey line* at 66-NDGD on given

side (respectively *right* and *left*). **c** Differences between sides of brain (*right* and *left*) for given NDGD (22, $\overline{22}$ and 66). *Black line* represents the *right side* and *grey line* the *left side* of the brain for given NDGD (respectively, 22 on the *left*, $\overline{22}$ in the *middle* and 66 on the *right*). *Red lines* indicate values in the *right side* which are higher than in the *left side* and *green lines* indicate the opposite. Differences are considered significant at $p < 0.05$ correcting using FDR

To better understand the results found for FA and MD, we performed the same analysis for individual eigenvalues λ_1 , λ_2 and λ_3 (Supplementary Figure S.4, S.5, and S.6).

Spatial distribution of the tract

A 2D Pearson correlation coefficient of the binarised tract (Fig. 5) showed a good level of correlation between tracts obtained using either $\overline{22}$ or 66 NDGDs (in the range 0.5 to

0.6) and as expected an even higher correlation between tracts obtained using either 22 or $\overline{22}$ NDGDs.

The mean Dice coefficient (\pm SD) between CST delineated with 22- and $\overline{22}$ -NDGD was 0.65 ± 0.09 for the right side and 0.68 ± 0.12 for the left side, and 0.53 ± 0.15 for the right and 0.57 ± 0.14 for the left when comparing CST delineated with $\overline{22}$ and 66-NDGDs.

Figure 6 reports the superimposition of all binarised tracts, which represents the spatial distribution of all tracts

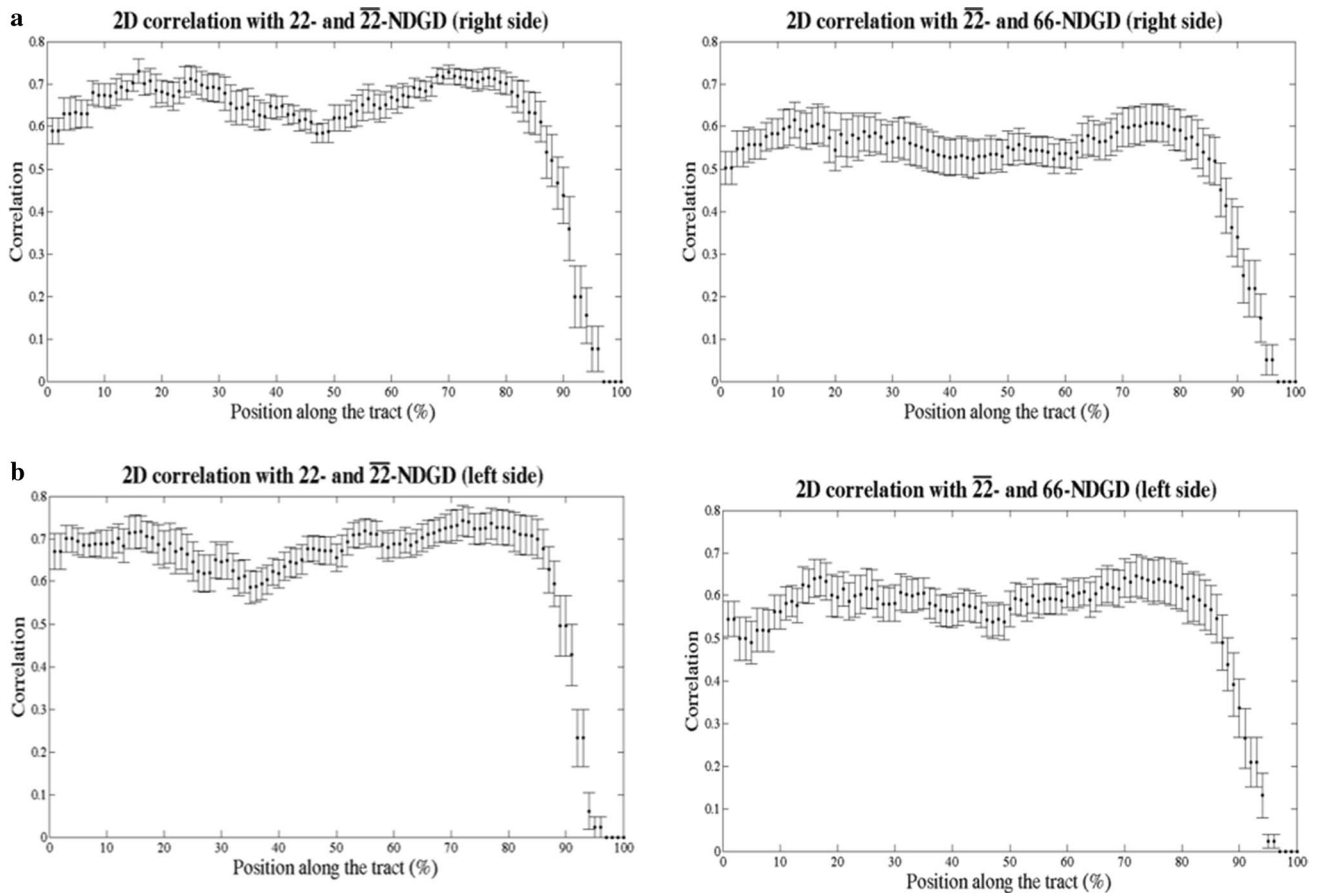


Fig. 5 Distribution along the tract of the Pearson correlation coefficient for right side (*left upper panel*) and left side (*left lower panel*) comparing 22 and $\overline{22}$ -NDGDs. Distribution along the tract of the

Pearson correlation coefficient for right side (*right upper panel*) and left side (*right lower panel*) comparing $\overline{22}$ and 66-NDGDs

volume. Results of the paired *t* test for COG of the x coordinate (COG_x), are reported in the Supplementary Materials comparing 22-NDGDs to $\overline{22}$ -NDGDs (Supplementary Figure S.7 panel A) and comparing $\overline{22}$ -NDGDs to 66-NDGDs (Supplementary Figure S.7 panel B). Results of the paired *t* test for the COG of the y coordinate (COG_y) are reported in the Supplementary Materials comparing 22-NDGDs to $\overline{22}$ -NDGDs (Supplementary Figure S.8 panel A) and comparing $\overline{22}$ -NDGDs to 66-NDGDs (Supplementary Figure S.8 panel B).

Crossing fibers analysis

Quantitative comparisons of the first fibers, and second fibers where present, were conducted performing a paired *t* test of the f1 and f2 volumes (Figs. 7 and Supplementary Figure S.9). The f1 and f2 volumes were greater at 66-NDGD than at $\overline{22}$ -NDGD along most of the tract for the f1 volume (Figure S.9 panel B) and along the entire tract for the f2 volume (Fig. 7, panel B). The greatest difference

was found in the f2 volume at 66-NDGD in the range of 45th–65th percentiles. This range was comparable to the central portion of the tract where FA has shown significant differences between $\overline{22}$ -NDGD and 66 NDGDs (Fig. 3b). No substantial difference was found in the f1 and f2 volumes between 22-NDGD and $\overline{22}$ -NDGD (Fig. 7a and Supplementary Figure S.9 panel A).

Discussion

In the present study, we investigated the effect of two acquisition protocols based on different number of diffusion gradient directions on MR diffusion parameters of the CST, reconstructed from diffusion data obtained from healthy subjects. To individuate the effects of different NDGDs, the protocols $\overline{22}$ - and 66-NDGDs differed only for this parameter.

Tracts were delineated applying the probabilistic tractography algorithm, *probtrackx2*, which tracked the CST

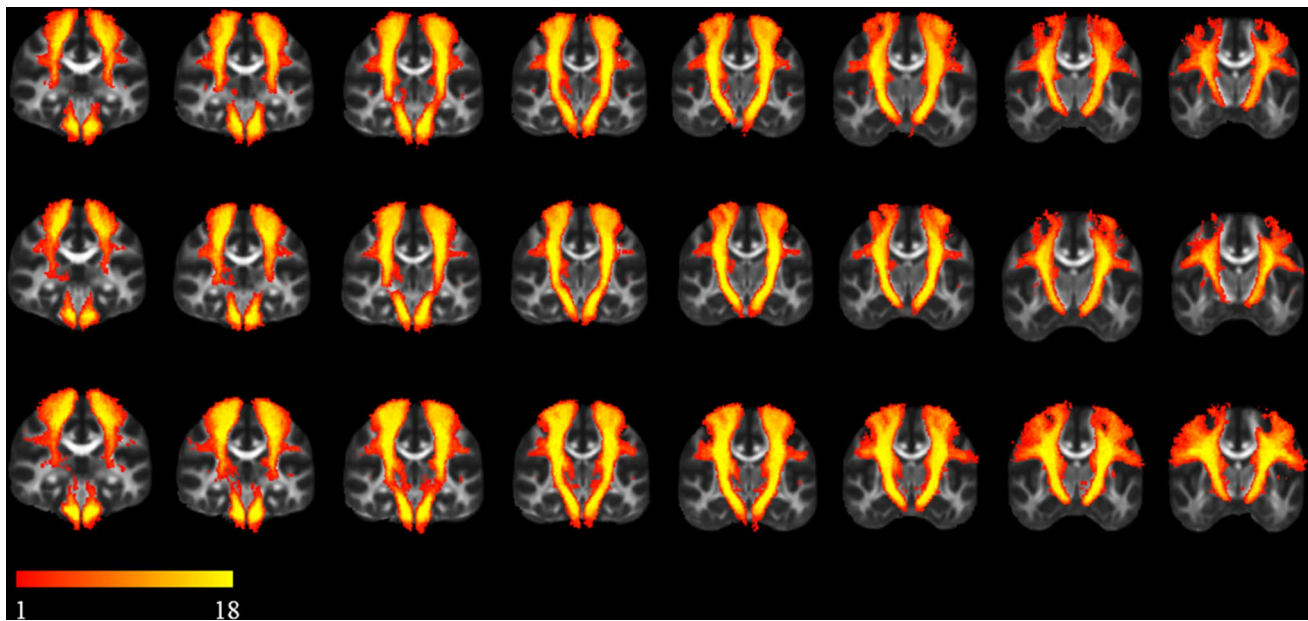


Fig. 6 Sum of binarised tracts of all subjects at 22-NDGD (*top*), $\overline{22}$ -NDGD (*middle*) and 66-NDGD (*bottom*) superimposed onto the mean FA template, views as successive slices. Intensity of this super-

position varies from 1 to 18 (total number of subjects). Color legend indicates *red* for minimum value of intensity and *yellow* for maximum value

from the primary motor cortex in the precentral gyrus to the pons. Other recent studies have also delineated the CST using similar anatomical location for ROIs [2, 33, 34]; our protocol varied in that we employed a Freesurfer segmentation mask of the primary motor cortex which automatically assures a subject specific seed; moreover, we drew the other ROIs on a study specific FA template. This procedure limits operator dependence and can be employed in studies with large numbers of subjects.

Some previous studies have investigated tract reconstruction and evaluated diffusion parameters along the tract using different approaches to parameterization [13, 14, 16, 35]. In order to improve regional specificity of the spatial statistics of the diffusion properties, we performed a division of each tract delineated into 100 segments for every subject, along the inferior-superior direction. FA values varied along the entire tract and across different subjects (Fig. 2). In addition, regional variability was significantly higher than subjects' whole-tract variability for both FA and MD values (Table 1). These results confirm the utility of performing an along-tract analysis, since a tract-average statistic could hide localized parameter differences [36]. The fact that the residual variances of both FA and MD are higher at 66-NDGDs with respect $\overline{22}$ -NDGDs suggests that a protocol with higher NDGDs is able to give spatial details of the tract accounting for a greater intra-subject variability.

In order to investigate specific regional differences along the tract, we compared each respective percentile between

subjects, using different NDGDs and for left and right hemispheres. Beyond the 90th percentile (Fig. 2), FA and MD values were found to be unreliable. Values beyond the 90th percentile were unreliable due the presence of liquor and meninges which increased apparent MD, while in the final few percentiles close the skull, DTI parameters were not reliably calculated.

The comparison of FA values at $\overline{22}$ -NDGDs and 66 NDGDs is particularly interesting (Fig. 3b). On the right side of the brain, FA values at $\overline{22}$ -NDGDs showed an increase immediately above the PLIC (50th–70th percentiles), while on the left side differences were present in a wider central region of the CST. To test the hypothesis that FA differences could be due to the presence of the second fiber, which was differentially detected by analyses using different NDGDs, we investigated the volume of the first and second detected fiber. For both sides of the brain, along most of the central portion of the tract for the first fiber (Supplementary Figure S.9), and along the most of the CST for the second fiber (Fig. 7), the volumes at 66-NDGD were higher respect to those at $\overline{22}$ -NDGDs.

In particular, differences in f2 volumes peaked at the level of the pons and of the 50th percentile, where the volume was tripled for the acquisition using 66 NDGDs. Differences in volume depended on the fact that for 66-NDGD data, the algorithm more readily detects dominant fiber directions beyond the first. Although the CST is one of the major descending white matter tracts in the human brain and its topographical localization at different levels has

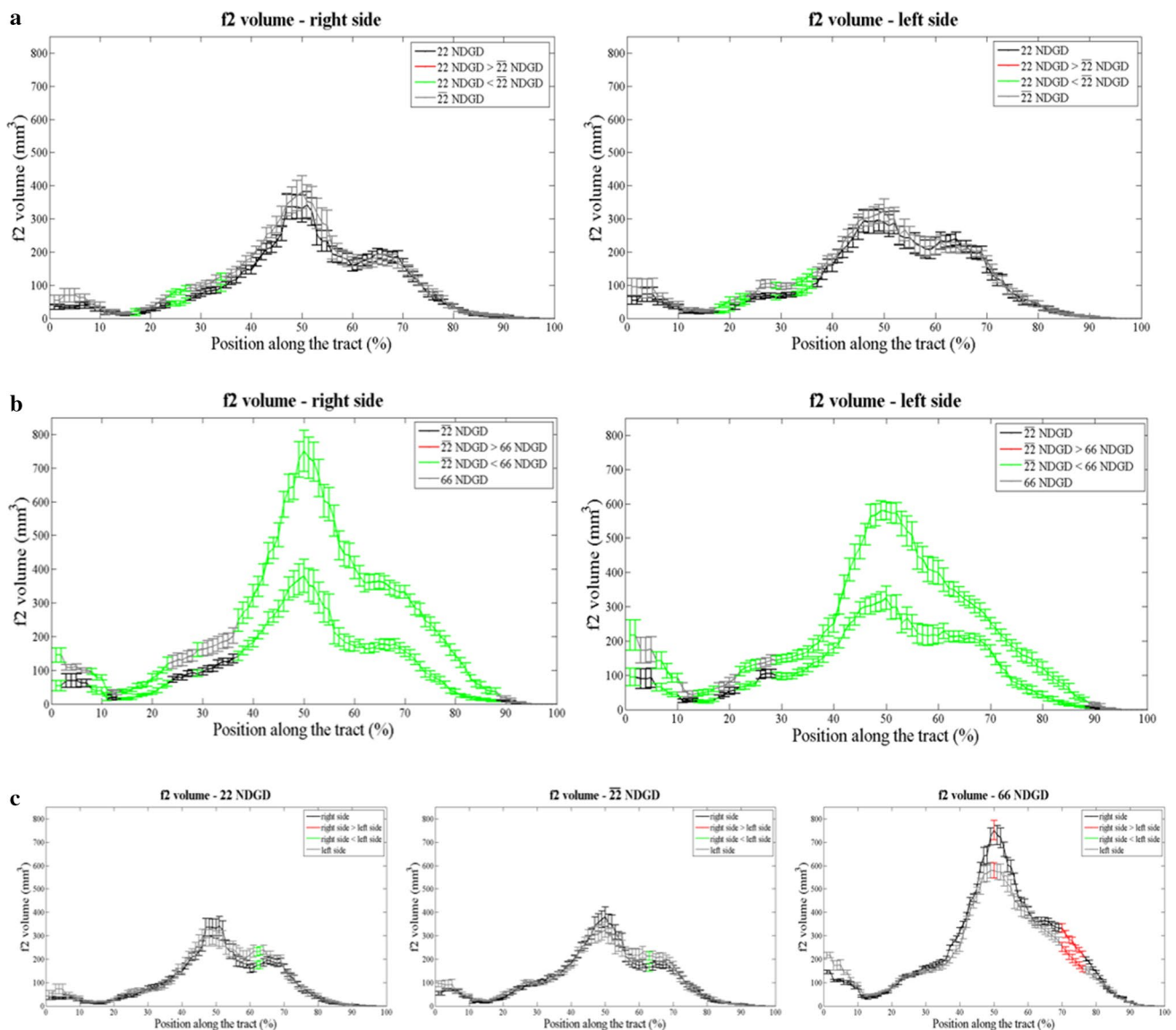


Fig. 7 Paired t test on f2 volume. From the *top*, **a** illustrates f2 volume distributions and differences between two NDGD (respectively, 22 and 22) on given side (*right* and *left*). *Black line* represents f2 volume at 22-NDGD, and *grey line* at 22-NDGD on given side (respectively *right* and *left*). *Red lines* indicate values at 22-NDGD which are higher than those at 22 and *green lines* indicate the opposite. **b** Illustrates f2 volume distributions and differences between 22-NDGD and 66-NDGDs. *Black line* represents f2 volume at 22-NDGD, and *grey*

line at 66-NDGD on given side (respectively *right* and *left*). **c** Differences between sides of brain (*right* and *left*) for given NDGD (22, 22 and 66). *Black line* represents the right side and *grey line* the left side of the brain for given NDGD (respectively, 22 on the *left*, 22 in the *middle* and 66 on the *right*). *Red lines* indicate values in the *right side* which are higher than in the *left side* and *green lines* indicate the opposite. Differences are considered significant at $p < 0.05$ correcting using FDR

been extensively studied, important issues regarding its in vivo reconstruction are still in debate. Previous MR and anatomical studies of human brain have shown that the portion of the CST passing through the corona radiata (corresponding to our 50th percentile) intersects other fasciculi, such as the superior longitudinal fasciculus, as well as fibers of the corpus callosum [37, 38]. In addition, it is known that the pons contains many crossing fibers corresponding

to the middle cerebellar peduncle, the pontine crossing tract (both in lateral orientation), the corticospinal tract (superior-inferior orientation), and the medial lemniscus [39]. The ability to resolve crossing fibers depends on diffusion models more complex than a tensor model. Specifically, it has been shown that tensor models are unable to visualize fibers of the CST crossing the arcuate fasciculus [40] while *bedpostx* can detect the projections of the CST to lateral

portions of the sensorimotor cortex [24] that may well be responsible for the major differences in the paired *t* test of the volume of the second fiber between 22 and 66-NDGD.

The decrease of FA values relative to diffusion data with a larger number of gradients has already been reported [22, 41, 42]. We interpreted the increase in FA at 22 NDGDs by considering that the second fiber detected by 22-NDGD acquisition has a volume substantially inferior to that detected by a 66-NDGD acquisition (Fig. 7b); this means that 66-NDGD acquisitions have a better sensitivity in detecting portions of the tract where different fiber orientations are present, thus leading to a decrease in average anisotropy values.

A comparison between different NDGDs for MD values showed no significant differences on either side of the brain (Fig. 4).

The along-tract analysis of eigenvalues is in line with results obtained for MD (Supplementary Figures S.3–S.5). Small portions of the tract show differences between 22-NDGDs and 66-NDGDs with opposing tendencies of λ_1 with respect to λ_2 and λ_3 that in combination do not generate significant difference in MD results.

Comparing protocols that differed only for SNR, fixing the number of gradient directions, namely 22- and 22-NDGDs, we observed no substantial differences in diffusion parameters (FA, f1 and f2 volume) and spatial characteristics of the CST between.

Considering differences between the left and right corticospinal tracts, plots of all three eigenvalues showed no left–right differences, in agreement with the analogous MD distribution, although we did find some significant differences in FA, f1 and f2 volumes using either the 22-NDGDs or the 66-NDGDs protocols, most notably higher FA values in the right lower portion of CST (at the level of pons and cerebral peduncle). The fact that the signs of asymmetry observed were at the level of the pons may reflect hemilateral differences in the proportion of fibers that form ipsi- and contralateral tracts in the decussation immediately below the pons [43]. While many studies have analyzed asymmetries of white matter tracts and in particular of CST, and their correlation with handedness, this issue is still debated in literature. Some studies have found that this asymmetry takes the form of a preponderance of corticospinal fibers in the right side of the spinal cord [44]. But other post-mortem [45] and in vivo tractography studies [40, 46] have found a leftward asymmetry in the precentral component of the pyramidal tract and arcuate fasciculus. Moreover, Herve et al. [47] found the existence of an asymmetry that is hand dominance-dependent in the precentral gyri, while other works, like the study of Westerhausen et al. [48], showed asymmetry of the corticospinal tract at the level of the internal capsule, but failed to demonstrate a direct correlation with hand dominance. We think that

a confirmation of any possible asymmetry of CST needs to be investigated with an isotropic, high-resolution DWI investigation with a greater number of subjects.

Many studies have analyzed the influence of NDGD on diffusion-weighted imaging, to optimize DWI acquisition, possibly in a clinical setting, where total scan time cannot be too long and diffusion measures have to be both robust and reasonably accurate. As is often the case, the findings are not unambiguous: some studies have found that the minimum NDGD (6) is sufficient or even optimal for measuring mean diffusivity and FA in the brain [49, 50]. Other researchers determine the minimum NDGD for robust estimation of FA to be 18–21 [51]. Simulation allows the appropriate number of diffusion gradient orientations to be calculated for accurate estimation of various diffusion metrics [22]. Few have investigated the effect of the NDGD on DTI measurements in vivo: Ni et al. [21] compared DW protocols with 6, 21, and 31 NDGD and found in a ROI based analysis that FA and MD were not significantly different among the three protocols, but there were significant differences in the values of eigenvalues. In particular λ_1 and λ_2 were higher and λ_3 was lower at 6-NDGD with respect to 21 and 31-NDGD. As far as we know, only one study has quantitatively estimated how diffusion measures related to specific tracts under evaluations changes with the number of diffusion gradients directions. Yao et al [52] assessed the effect of different NDGD (6, 11, 21, and 31) on diffusion tensor fiber tracking, using a deterministic algorithm for tractography and an averaged analysis for the tracts they chose to delineate. By visual assessment, they found that protocols with higher NDGD gave better tracking results, while concerning the diffusion-averaged measurements all parameter values were significantly greater at 6-NDGD than those with the other NDGDs, apart from average tract length which proved to be significantly smaller. The authors assert that one limitation of the study was the inability to distinguish pathways in voxels that contain crossing fibers.

In addition to the effects of NDGD in an along-tract tractography analysis of the CST, we also investigated the spatial correlation of CSTs obtained at 22-NDGDs with respect to 66-NDGDs. Figure 6 shows the distribution of all superimposed tracts and highlights the close correspondence among subjects and between different NDGD data sets. The major difference is at the level of the projection of CST to the lateral portions of the sensorimotor cortex.

The Dice coefficient showed a concordance between tracts obtained at different NDGD which ranged from moderate to good. Similarly, performing a 2D spatial comparison, we observed a Pearson correlation coefficient in a range between 0.5 and 0.7. Overall, the spatial correlation is better between 22-NDGD and 22-NDGDs than the correlation between 22-NDGDs and 66-NDGD, as expected.

While the spatial correlation results demonstrated the reliability of the CST obtained at 22-NDGD, the f2 volume distributions confirm the evidence of a greater number of fibers detected at 66-NDGD. In particular, this is apparent in the lateral portion of the CST which is not completely described by the first fiber alone.

Overall, 66-NDGD proved to be superior in CST reconstruction and also shows a good absolute level of performance for tractography reconstruction. However, the good spatial correspondence between tracts delineated with 22-NDGD and 66-NDGD suggests that the 22-NDGD protocol may be suitable for clinical studies, when a short scan time is often needed.

Further spatial analyses were performed: the COG for x and y showed that the tracts delineated at 66-NDGD were somewhat more mesial (significant differences in COG x distribution for the right side, Supplementary Figure S.8) and more anterior (significant differences for COG y , Supplementary Figure S.9) compared to those at 22-NDGDs.

This study has some limitations: the intensity of the static magnetic field (1.5 T) and the performance of the gradient system on our clinical scanner determines not only the limited spatial resolution, but also the relatively long duration of the acquisition time. Although our study is based on a well-established tractography algorithm, our results may have been affected by the spatial resolution and non-isotropic form of the voxel we used.

Another limitation is the voxel dimension employed: both a more isotropic form and reduced dimensions could improve the quality of tractography reconstruction.

Conclusion

In summary, in this study we applied an along-tract analysis of diffusion parameters in the CST defined by a semi-automatic procedure, to assess the effect of different NDGDs on a probabilistic tractography approach, which is particularly powerful in evaluating crossing fibers when present. The developed methodology offers a tool for tractography analysis both for research and clinical studies. Our work provides an example of a comparison of tractography results obtained using data from two schemes of acquisitions which can be used with a clinical scanner. The along-tract analysis we performed demonstrates the differences in the CST definition with such different acquisition schemes (mostly due to NDGDs and acquisition time). These results should aid in the choice of the most suitable protocol to be used depending on the clinical question, balancing the need to have the most accurate definition of the CST tract (for example in the pre-surgical evaluation of brain lesions) with the need to analyze the properties of the CST tract in a short acquisition time (for example in the

evaluation of neurodegenerative diseases which may affect the whole tract).

Acknowledgements We thank Claudio Bianchini for technical assistance.

Compliance with ethical standards

Conflict of interest The authors declare that they have no conflict of interest.

Ethical standards All procedures performed in studies involving human participants were in accordance with the ethical standards of the institutional research committee and with the 1964 Helsinki declaration and its later amendments.

Informed consent Informed consent was obtained from all individual participants included in the study.

References

- Mori S, van Zijl PC (2002) Fiber tracking: principles and strategies—a technical review. *NMR Biomed* 15:468–480
- Ciccarelli O, Behrens TE, Altmann DR, Orrell RW, Howard RS, Johansen-Berg H, Miller DH, Matthews PM, Thompson AJ (2006) Probabilistic diffusion tractography: a potential tool to assess the rate of disease progression in amyotrophic lateral sclerosis. *Brain* 129:1859–1871
- Bastin ME, Pettit LD, Bak TH, Gillingwater TH, Smith C, Abrahams S (2013) Quantitative tractography and tract shape modeling in amyotrophic lateral sclerosis. *J Magn Reson Imaging* 38(5):1140–1145
- Mori S, Crain B, Chacko VP, van Zijl PCM (1999) Three dimensional tracking of axonal projections in the brain by magnetic resonance imaging. *Ann Neurol* 45:265–269
- Basser PJ, Pajevic S, Pierpaoli C, Duda J, Aldroubi A (2000) In vivo fiber tractography using DT-MRI data. *Magn Reson Med* 44:625–632
- Wahl M, Li YO, Ng J, Lahue SC, Cooper SR, Sherr EH, Mukherjee P (2010) Microstructural correlations of white matter tracts in the human brain. *Neuroimage* 51(2):531–541
- Tournier JD, Calamante F, Connelly A (2012) MRtrix: diffusion tractography in crossing fiber regions. *Int J Imag Syst Tech* 22(1): 53–66
- Garyfallidis E, Brett M, Amirbekian B, Rokem A, Van Der Walt S, Descoteaux M, Nimmo-Smith I (2014) Dipy, a library for the analysis of diffusion MRI data. *Front Neuroinform* 8:1–17
- Jones DK, Knösche TR, Turner R (2013) White matter integrity, fiber count, and other fallacies: the do's and don'ts of diffusion MRI. *Neuroimage* 73:239–254
- Pujol S, Wells W, Pierpaoli C, Brun C, Gee J, Cheng G, Vemuri B, Commowick O, Prima S, Stamm A, Goubran M, Khan A, Peters T, Neher P, Maier-Hein KH, Shi Y, Tristan-Vega A, Veni G, Whitaker R, Styner M, Westin CF, Gouttard S, Norton I, Chauvin L, Mamata H, Gerig G, Nabavi A, Golby A, Kikinis R (2015) The DTI challenge: toward standardized evaluation of diffusion tensor imaging tractography for neurosurgery. *J Neuroimaging* 25(6): 875–882
- O'Donnell LJ, Westin CF, Golby AJ (2009) Tract-based morphometry for white matter group analysis. *Neuroimage* 45(3):832–844

12. Gong G, Jiang T, Zhu C, Zang Y, Wang F, Xie S, Xiao J, Guo X (2005) Asymmetry analysis of cingulum based on scale-invariant parameterization by diffusion tensor imaging. *Hum Brain Mapp* 24(2):92–98
13. Lin F, Yu C, Jiang T, Li K, Li X, Qin W, Sun H, Chan P (2006) Quantitative analysis along the pyramidal tract by length-normalized parameterization based on diffusion tensor tractography: application to patients with relapsing neuromyelitis optica. *Neuroimage* 33(1):154–160
14. Reich DS, Smith SA, Jones CK, Zackowski KM, van Zijl PC, Calabresi PA, Mori S (2006) Quantitative characterization of the corticospinal tract at 3T. *AJNR Am J Neuroradiol* 27(10):2168–2178
15. Oh JS, Song IC, Lee JS, Kang H, Park KS, Kang E, Lee DS (2007) Tractography-guided statistics (TGIS) in diffusion tensor imaging for the detection of gender difference of fiber integrity in the midsagittal and parasagittal corpora callosa. *Neuroimage* 36:606–616
16. Oh JS, Kubicki M, Rosenberger G, Bouix S, Levitt JJ, McCarley RW, Westin CF, Shenton ME (2009) Thalamo-frontal white matter alterations in chronic schizophrenia: a quantitative diffusion tractography study. *Hum Brain Mapp* 30(11):3812–3825
17. Hong JH, Son SM, Jang SH (2010) Somatotopic location of corticospinal tract at pons in human brain: a diffusion tensor tractography study. *Neuroimage* 51:952–955
18. Hong YH, Lee KW, Sung JJ, Chang KH, Song IC (2004) Diffusion tensor MRI as a diagnostic tool of upper motor neuron involvement in amyotrophic lateral sclerosis. *J Neurol Sci* 227:73–78
19. Toosy AT, Werring DJ, Orrell RW, Howard RS, King MD, Barker GJ et al (2003) Diffusion tensor imaging detects corticospinal tract involvement at multiple levels in amyotrophic lateral sclerosis. *J Neurol Neurosurg Psychiatry* 74:1250–1257
20. Abe O, Yamada H, Masutani Y, Aoki S, Kunimatsu A, Yamasue H, Fukuda R, Kasai K, Hayashi N, Masumoto T et al (2004) Amyotrophic lateral sclerosis: diffusion tensor tractography and voxelbased analysis. *NMR Biomed* 17:411–416
21. Ni H, Kavcic V, Zhu T, Ekholm S, Zhong J (2006) Effects of number of diffusion gradient directions on derived diffusion tensor imaging indices in human brain. *AJNR Am J Neuroradiol* 27:1776–1781
22. Jones D (2004) The Effect of gradient sampling schemes on measures derived from diffusion tensor MRI: a Monte Carlo study. *Magn Reson Med* 51:807–815
23. Landman BA, Farrell JA, Jones CK, Smith SA, Prince JL, Mori S (2007) Effects of diffusion weighting schemes on the reproducibility of DTI-derived fractional anisotropy, mean diffusivity, and principal eigenvector measurements at 1.5T. *Neuroimage* 36(4):1123–1138
24. Lebel C, Benner T, Beaulieu C (2012) Six is enough? Comparison of diffusion parameters measured using six or more diffusion-encoding gradient directions with deterministic tractography. *Magn Reson Med* 68(2):474–483
25. Behrens T, Johansen Berg H, Jbabdi S, Rushworth M, Woolrich M (2007) Probabilistic diffusion tractography with multiple fibre orientations: what can we gain? *NeuroImage* 34:144–155
26. Oldfield RC (1971) The assessment and analysis of handedness: the Edinburgh inventory. *Neuropsychologia* 9:97–113
27. Jenkinson M, Smith SM (2001) A global optimisation method for robust affine registration of brain images. *Med Image Anal* 5(2):143–156
28. Ardekani BA, Braun M, Hutton BF, Kanno I, Iida H (1995) A fully automatic multimodality image registration algorithm. *J Comput Assist Tomogr* 19(4):615–623
29. Fischl B (2012) FreeSurfer. *Neuroimage* 62(2):774–781
30. Smith SM, Jenkinson M, Johansen-Berg H, Rueckert D, Nichols TE, Mackay CE, Watkins KE, Ciccarelli O, Cader MZ, Matthews PM et al (2006) Tract-based spatial statistics: voxelwise analysis of multi-subject diffusion data. *Neuroimage* 31:1487–1505
31. Anderson VM, Wheeler-Kingshott CA, Abdel-Aziz K, Miller DH, Toosy A, Thompson AJ, Ciccarelli O (2011) A comprehensive assessment of cerebellar damage in multiple sclerosis using diffusion tractography and volumetric analysis. *Mult Scler* 17(9):1079–1087
32. Guye M, Parker GJ, Symms M, Boulby P, Wheeler-Kingshott CA, Salek-Haddadi A, Barker GJ, Duncan JS (2003) Combined functional MRI and tractography to demonstrate the connectivity of the human primary motor cortex in vivo. *Neuroimage* 19(4):1349–1360
33. Yasmin H, Aoki S, Abe O, Nakata Y, Hayashi N, Masutani Y, Goto M, Ohtomo K (2009) Tract-specific analysis of white matter pathways in healthy subjects: a pilot study using diffusion tensor MRI. *Neuroradiology* 51:831–840
34. Hattori T, Yuasa T, Aoki S, Sato R, Sawaura H, Mori T, Mizusawa H (2011) Altered microstructure in corticospinal tract in idiopathic normal pressure hydrocephalus: comparison with Alzheimer Disease and Parkinson Disease with dementia. *AJNR Am J Neuroradiol* 32:1681–1687
35. Surova Y, Szczepankiewicz F, Lätt J, Nilsson M, Eriksson B, Leemans A, Hansson O, van Westen D, Nilsson C (2013) Assessment of global and regional diffusion changes along white matter tracts in parkinsonian disorders by MR tractography. *PLoS One* 8(6):e66022
36. Colby J, Soderberg L, Lebel C, Dinova I, Thompson P, Sowell E (2012) Along-tract statistics allow for enhanced tractography analysis. *Neuroimage* 59(4):3227–3242
37. Holodny AI, Watts R, Korneenko VN, Pronin IN, Zhukovskiy ME, Gor DM, Ulug A (2005) Diffusion tensor tractography of the motor white matter tracts in man: Current controversies and future directions. *Ann N Y Acad Sci* 1064:88–97 (**Review**)
38. Jellison BJ, Field AS, Medow J, Lazar M, Salamat MS, Alexander AL (2004) Diffusion tensor imaging of cerebral white matter: a pictorial review of physics, fiber tract anatomy, and tumor imaging patterns. *AJNR Am J Neuroradiol* 25(3):356–369
39. King MD, Gadian DG, Clark CA (2009) A random effects modelling approach to the crossing-fibre problem in tractography. *Neuroimage* 44(3):753–768
40. Thiebaut de Schotten M, Ffytche DH, Bizzi A, Dell'Acqua F, Allin M, Walshe M, Murray R, Williams SC, Murphy DG, Catani M (2011) Atlasing location, asymmetry and inter-subject variability of white matter tracts in the human brain with MR diffusion tractography. *Neuroimage* 54(1):49–59
41. Jones DK, Cercignani M (2010) Twenty-five pitfalls in the analysis of diffusion MRI data. *NMR Biomed* 23(7):803–820
42. Barrio-Arnanz G, de Luis-García R, Tristán-Vega A, Martín-Fernández M, Aja-Fernández S (2015) Impact of MR acquisition parameters on DTI scalar indexes: a tractography based approach. *PLoS One* 10(10):e0137905
43. Al Masri O (2011) An essay on the human corticospinal tract: history, development, anatomy, and connections. *Neuroanatomy* 10:1–4
44. Nathan PW, Smith MC, Deacon P (1990) The corticospinal tracts in man. Course and location of fibres at different segmental levels. *Brain* 113:303–324
45. Rademacher J, Bürgel U, Geyer S, Schormann T, Schleicher A, Freund HJ, Zilles K (2001) Variability and asymmetry in the human precentral motor system. A cytoarchitectonic and myeloarchitectonic brain mapping study. *Brain* 124(Pt 11):2232–2258
46. Lebel C, Beaulieu C (2009) Lateralization of the arcuate fasciculus from childhood to adulthood and its relation to cognitive abilities in children. *Hum Brain Mapp* 30(11):3563–3573

47. Herve PY, Leonard G, Perron M, Pike B, Pitiot A, Richer L, Veillette S, Pausova Z, Paus T (2009) Handedness, motor skills and maturation of the corticospinal tract in the adolescent brain. *Hum Brain Mapp* 30:3151–3162
48. Westerhausen R, Huster RJ, Kreuder F, Wittling W, Schweiger E (2007) Corticospinal tract asymmetries at the level of the internal capsule: is there an association with handedness? *Neuroimage* 37: 379–386
49. Papadakis NG, Xing D, Houston GC, Smith JM, Smith MI, James MF, Parsons AA, Huang CL, Hall LD, Carpenter TA (1999) A study of rotationally invariant and symmetric indices of diffusion anisotropy. *Magn Reson Imaging* 17(6):881–892
50. Skare S, Hedehus M, Moseley ME, Li TQ (2000) Condition number as a measure of noise performance of diffusion tensor data acquisition schemes with MRI. *J Magn Reson* 147(2):340–352
51. Papadakis NG, Murrills CD, Hall LD, Huang CL, Adrian Carpenter T (2000) Minimal gradient encoding for robust estimation of diffusion anisotropy. *Magn Reson Imaging* 18(6):671–679
52. Yao X, Yu T, Liang B, Xia T, Huang Q, Zhuang S (2015) Effect of increasing diffusion gradient direction number on diffusion tensor imaging fiber tracking in the human brain. *Korean J Radiol* 16(2):410–418